Smart Mater. Struct. 7 (1998) 189–198. Printed in the UK PII: S0964-1726(98)90267-1

Simultaneous displacement and temperature sensing using a white light interrogated low finesse cavity in line with a fiber Bragg grating

L A Ferreira†‖, A B Lobo Ribeiro†, J L Santos†‡ and F Farahi§¶

† Grupo de Optoelectrónica, INESC, Rua do Campo Alegre, 687, 4150 Porto, Portugal
‡ Departamento de Física, Universidade do Porto, Ruo do Campo Alegre, 687, 4150 Porto, Portugal
§ Department of Physics, University of North Carolina, Charlotte, North Carolina 28223, USA

Received 16 October 1996, accepted for publication 9 July 1997

Abstract. A fiber optic sensing system for simultaneous measurement of displacement and temperature is presented. It is based on the use of a low finesse extrinsic Fabry–Pérot cavity and a fiber Bragg grating for temperature compensation. A white light tandem interferometric technique is used to recover the signal from the low finesse cavity, providing both fringe visibility and phase measurements. These, together with the fiber grating signal, give two equations that can be used to simultaneously determine temperature and displacement. Theoretical analysis of the sensing scheme is performed. Experimental results are presented which validate theoretical predictions and also demonstrate the feasibility of this sensing system in practical applications.

1. Introduction

In the field of fiber optic sensors, the use of a low finesse cavity as the sensing element has been shown to be an attractive solution for monitoring several physical measurands in situations when a small sensor is required and the measurements are made at remote locations [1, 2]. An extrinsic low finesse cavity with its simple design and small dimensions meets these requirements. However, in many situations where the primary measurand is displacement, undesirable temperature sensitivity can compromise its operation. This effect can, to some extent, be minimized by using materials with low thermal expansion coefficient for the external cavity [3]. A more attractive solution would be a sensor topology that monitors temperature while measuring displacement, and hence simultaneously obtains information corresponding to the two measurands [4]. The advantages of this approach are evident, namely, to reduce the constraints on the fabrication of the external cavity, and to measure the local temperature which is important in various applications.

The subject of simultaneous measurement of several quasi-static parameters has been an active research topic in the past few years [5–7]. With the advent of the fiber Bragg grating, this research area has become even more attractive [8, 9] and fiber optic sensors based on these elements have been developed to measure strain and temperature in civil structures and composites [10–16]. In this work we present a sensor topology which combines a low finesse cavity and a fiber Bragg grating. This grating provides a localized temperature reference for a cavity designed to work as a displacement sensor, although it is intrinsically sensitive to temperature. Therefore, the proposed sensing configuration allows the simultaneous measurement of displacement and temperature which are two important parameters to be monitored in smart structure applications. Also, the architecture of the sensor head described below is compatible with small size and localized measurement, which are significant features in this field.

2. Theory

The schematic of the sensing system is shown in figure 1. A Fabry–Pérot cavity is formed between the fiber end and a mirror. Generally, the low reflection from the fiber end (due to the small mismatch between the indices of refraction) and the low level of light being collected back from the mirror to the fiber (due to the cavity length and absence of any lens) make this cavity a low finesse one, with a

‖ Phone: +351 2 2094327, fax: +351 2 2008487, email: lferreir@goe.inescn.pt
¶ Phone: (704) 547-2818, fax: (704) 547-3160, email: ffarahi@uncc.edu

transfer function similar to a two beam interferometer. The light source used to illuminate the system has a coherence length much smaller than the cavity length, so that an interferometric signal is only recovered when the path imbalance of the receiving Mach–Zehnder is adjusted to the cavity length ($L_{INT} = 2L_{CAV}$). This means that a white light tandem interferometric technique is used to detect displacement of the cavity mirror. To measure temperature variations in the cavity, a sensing fiber Bragg grating sensor (FBG_S) is placed near the fiber end. In this configuration, the sensing grating is only affected by temperature change within the cavity (ΔT), while the interferometric signal is affected by temperature variation in the cavity (ΔT) and by the mirror displacement (ΔL_M). Another fiber Bragg grating (FBG_R) is placed near the receiving Mach–Zehnder interferometer. This grating is actively tuned such that its spectral response matches the spectral response of the sensing grating, preventing light within the spectrum of the gratings from reaching the receiving interferometer. If, due to temperature variations in the cavity, the Bragg wavelength of the sensing grating changes, the detected optical power in Out_2 will decrease due to the mismatch between the spectral responses of both sensing and receiving gratings. To maximize the power, the fiber containing the receiving grating is stretched to once again match the spectral response of two gratings. Therefore, a change in the Bragg wavelength of the sensing grating originated by a temperature variation is compensated by a change in the Bragg wavelength of the receiving grating produced by applied strain. Because, in general, the relations between the Bragg wavelength and temperature, and between the Bragg wavelength and strain are both linear, the applied signal to the receiving fiber Bragg grating is directly proportional to the temperature change at the sensor location, i.e.,

$$\Delta S_{FBG} = K_{T/FBG}\Delta T. \tag{1}$$

In this equation, ΔS_{FBG} is the elongation of the fiber containing the FBG_R required to keep it tuned to the FBG_S and $K_{T/FBG}$ is a coefficient that depends on the fiber grating characteristics and also on the length of the elongated fiber. This means that, due to active compensation, the optical power at Out_2 will be always maximum. In the following, the optical power arriving at detector D_2 will be calculated.

The spectral power density emitted by the source, $P_S(\nu)$, can be written as:

$$P_S(\nu) = \frac{2P_0}{\Delta\nu_S}\sqrt{\frac{\ln 2}{\pi}}\,\mathrm{e}^{-4\ln 2\left(\frac{\nu-\nu_0}{\Delta\nu_S}\right)^2} \tag{2}$$

where P_0 is the total power injected in the fiber, $\Delta\nu_S$ is the FWHM of the assumed Gaussian spectrum for the optical source and ν_0 is its central frequency. The spectral response of the fiber Bragg gratings can be written as:

$$FBG(\nu) = R\,\mathrm{e}^{-4\ln 2\left(\frac{\nu-\nu_B}{\delta\nu}\right)^2} \tag{3}$$

where it is assumed that the Gaussian has profiles with FWHM $\delta\nu$, reflectivity R ($0 \le R \le 1$) and Bragg frequency of ν_B (for simplicity, both gratings, FBG_S and FBG_R are considered similar). When the effective reflection from the mirror, and from the fiber end are both small, the transfer function of the cavity would be similar to a two beam interferometer. In this analysis we assume these coefficients are equal and $k \ll 1$. Therefore [2],

$$CAV(\nu) = 2k\left[1+\cos\left(\frac{2\pi\nu}{c}\left(2L_{CAV}+2\Delta L_{CAV}\right)\right)\right]. \tag{4}$$

In the above equation, c is the speed of light, L_{CAV} is a fixed value for the cavity length and $\Delta L_{CAV} = \Delta L_M + \Delta L_T$, where ΔL_{CAV} is the variation of the cavity length, ΔL_M is the term representing the mirror displacement and ΔL_T is associated with thermal effects in the cavity ($\Delta L_T = \beta\Delta T$). The spectral power density reflected by the receiving grating to detector D_2 can now be written as:

$$P_2(\nu) = \frac{1}{16}P_S(\nu)FBG^2(\nu) + \frac{1}{16}P_S(\nu)[1-FBG(\nu)]^2FBG(\nu)CAV(\nu). \tag{5}$$

From this equation, the total power incident on the detector is given by:

$$P_2 = \int P_2(\nu)\,\mathrm{d}\nu. \tag{6}$$

The calculation of the integral is performed considering two approximations. (i) In equations containing $FBG(\nu)$, the spectral power density of the optical source is assumed constant and equal to the power at the Bragg frequency $P_S(\nu) = P_S(\nu_B)$. This approximation is valid since $\Delta\nu_S \gg \delta\nu$. (ii) Exponential terms of the form $\exp[-(L_{CAV}/L_{cFBG})^2]$ are considered unitary since, in general, $L_{cFBG} \gg L_{CAV}$ where

$$L_{cFBG} = \frac{c}{\delta\nu}\sqrt{\frac{2\ln 2}{\pi}} \tag{7}$$

is the coherence length of light reflected by the fiber Bragg grating. Under these approximations, from equations (5) and (6) we get:

$$P_2 = \frac{1}{16}\frac{R^2}{\sqrt{2}}P_0\frac{\delta\nu}{\Delta\nu_S}\,\mathrm{e}^{-4\ln 2\left(\frac{\nu_B-\nu_0}{\Delta\nu_S}\right)^2} + \frac{Rk}{4}\left(\frac{1}{2}-\frac{R}{\sqrt{2}}+\frac{R^2}{2\sqrt{3}}\right)P_0\frac{\delta\nu}{\Delta\nu_S}\,\mathrm{e}^{-4\ln 2\left(\frac{\nu_B-\nu_0}{\Delta\nu_S}\right)^2} \times\left[1+\cos\left(\frac{2\pi\nu_B}{c}\left(2L_{CAV}+2\Delta L_{CAV}\right)\right)\right]. \tag{8}$$

The two terms in this equation have the following physical interpretation. The first one is a DC term and results from the reflection of light in both gratings when they are tuned. The temperature of the sensor head can be obtained from the signal required to keep this value constant. The second term is the interference term which shows the optical signal returning from the cavity has been narrowly filtered by the receiving Bragg grating. Clearly, the amplitude of this term should be much smaller than the DC term for such a sensor to be valuable. However, this term does not fade out even when $R = 1$, because this reflectivity only happens at the Bragg frequency. In a case where $R \approx 1$ and $k \approx 0.04$, the amplitude of the interferometric term is nearly 50 times smaller than the DC one. Therefore, this interference can be

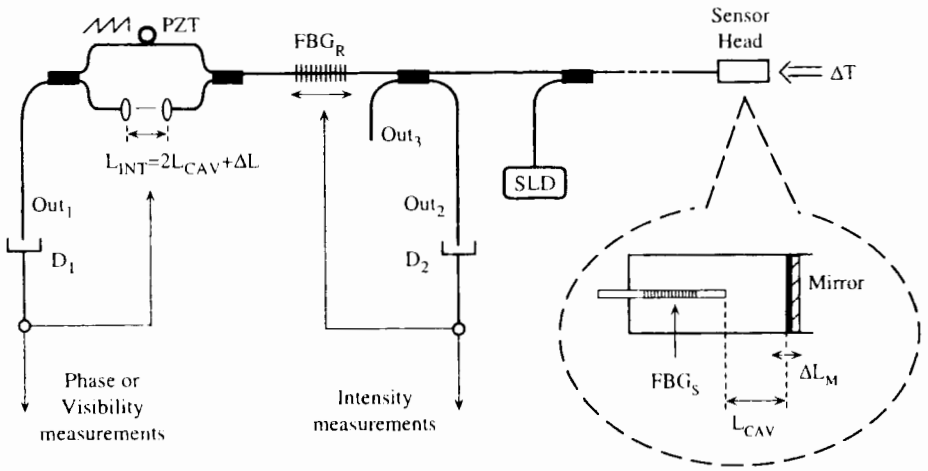

Figure 1. Proposed sensing system.

considered as a source of noise. To completely eliminate this contribution, a sensor Bragg grating with a spectral response larger than the receiver Bragg grating must be used. But, this will lead to a lower resolution in measuring ΔT. Therefore, in practice, the optimum ratio between these terms is determined based on the required resolution in measuring ΔT.

We will now consider the optical power arriving at detector D_1. Assuming a lossless system and couplers in the receiving interferometer with nominal coupling ratios of 1/2, the transfer function can be written as:

$$INT(\nu) = \frac{1}{2}\left[1 + \cos\left(\frac{2\pi\nu}{c}(2L_{CAV} + \Delta L)\right)\right] \quad (9)$$

where ΔL is the path imbalance of the white light tandem interferometer (difference between the cavity length and the path imbalance of the receiving interferometer). Using this function and equations (3) and (4), the spectral power density at Out_1 is given by:

$$P_1(\nu) = \frac{1}{8}P_S(\nu)[1 - FBG(\nu)]^3 CAV(\nu)INT(\nu) + \frac{1}{8}P_s(\nu)FBG(\nu)[1 - FBG(\nu)]INT(\nu). \quad (10)$$

It is convenient to split this equation in three terms:

$$\left.\begin{aligned} P_1(\nu) &= \frac{1}{8}P_S(\nu)CAV(\nu)INT(\nu)\Big\}A \\ &\left.\begin{aligned} &-\frac{3}{8}P_S(\nu)FBG(\nu)CAV(\nu)INT(\nu) \\ &+\frac{3}{8}P_S(\nu)FBG^2(\nu)CAV(\nu)INT(\nu) \\ &-\frac{1}{8}P_S(\nu)FBG^3(\nu)CAV(\nu)INT(\nu) \end{aligned}\right\} B \\ &\left.\begin{aligned} &+\frac{1}{8}P_S(\nu)FBG(\nu)INT(\nu) \\ &-\frac{1}{8}P_S(\nu)FBG^2(\nu)INT(\nu). \end{aligned}\right\} C \end{aligned} \quad (11)$$

Term A gives the equation correspondent to the case of a common white light tandem interferometer without fiber Bragg gratings. Term B is related to the portion of light in the spectral range of the gratings that reaches the cavity and then illuminates the receiving interferometer. Term C is due to the light in the spectral range of the gratings that will not reach the cavity but illuminates the receiving interferometer. Later, we will see that the amplitudes of the signal corresponding to all the terms in equation (11) relative to the signal represented by term A are very small. Therefore, we now concentrate only on this signal.

Figure 2 shows the spectrum of the signal arriving at detector D_1 when the receiving interferometer is tuned to the cavity ($\Delta L = 0$) and $L_{CAV} = 100\ \mu$m. These refer to three different situations: $\Delta L_{CAV} = 0$, $\Delta L_{CAV} = \lambda_0/8$ and $\Delta L_{CAV} = \lambda_0/4$ (λ_0 is the optical source central wavelength, correspondent to ν_0; for further comparison with experimental results, in these pictures we use λ instead of ν; $\lambda = c/\nu$). From this figure, it can be seen that the average power, which is obtained by integrating term A of equation (11), is maximum when the transfer function of the cavity is adjusted with the transfer function of the receiving interferometer. This means that the receiving interferometer acts as a filter on a channeled spectrum with the same spectral periodicity. When the cavity mirror moves, a modulation will appear at D_1 due to the match and mismatch of the filter and the channeled spectrum. This will not be the case when the filter and the channeled spectrum have different periodicity. In this situation, the spectral power density given by term A in equation (11) changes only its form when the cavity mirror moves, i.e., no power modulation will occur (this is equivalent to saying that no interference is visible at the output of the tandem interferometer). This can be confirmed in figure 3, which shows again the spectrum of the signal arriving at D_1 for $L_{CAV} = 100\ \mu$m, but now in the case when the receiving interferometer is not tuned to the cavity ($\Delta L = 50\ \mu$m). It can be observed that the total power given by the integration of the spectral power density does not depend on the position of the mirror (represented in the figure are the cases $\Delta L_{CAV} = 0$, $\Delta L_{CAV} = \lambda_0/8$ and $\Delta L_{CAV} = \lambda_0/4$). We should point out here that in figure 2, the values of P_1 for $\Delta L_{CAV} = 0$ and $\Delta L_{CAV} = \lambda_0/4$ indicate a fringe visibility of 1/2, as expected from a white light based system.

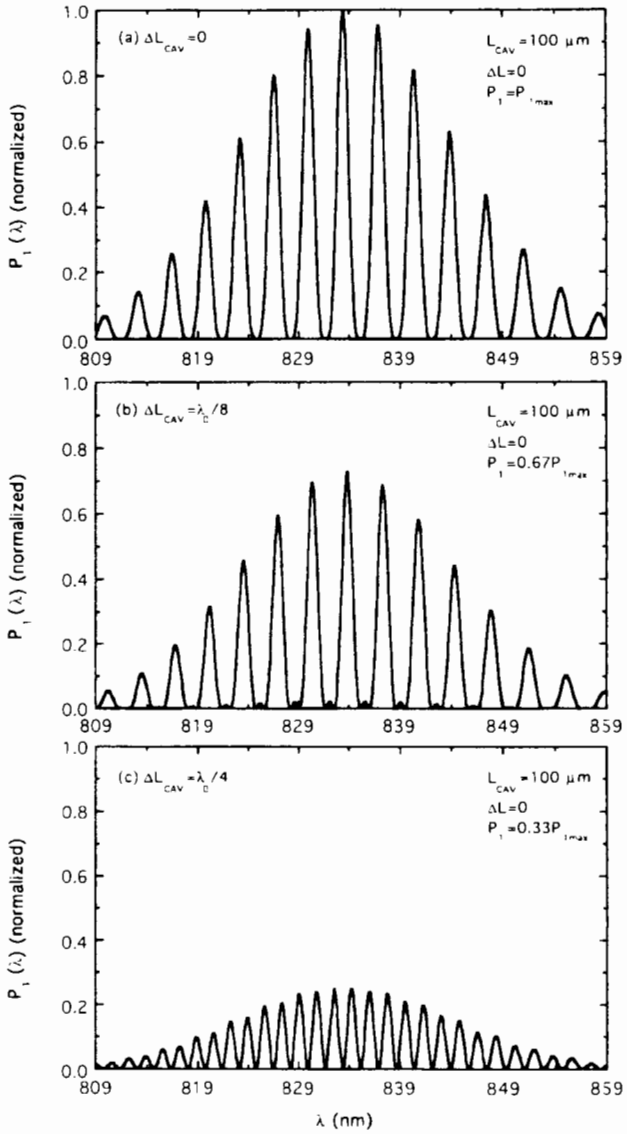

Figure 2. Normalized representation of term A of $P_1(\lambda)$ in equation (11) when $\Delta L = 0$ for three different situations: (a) $\Delta L_{CAV} = 0$; (b) $\Delta L_{CAV} = \lambda_0/8$; (c) $\Delta L_{CAV} = \lambda_0/4$ ($\lambda_0 = 833.5$ nm, $\Delta\lambda_S = 25$ nm, $L_{CAV} = 100$ μm).

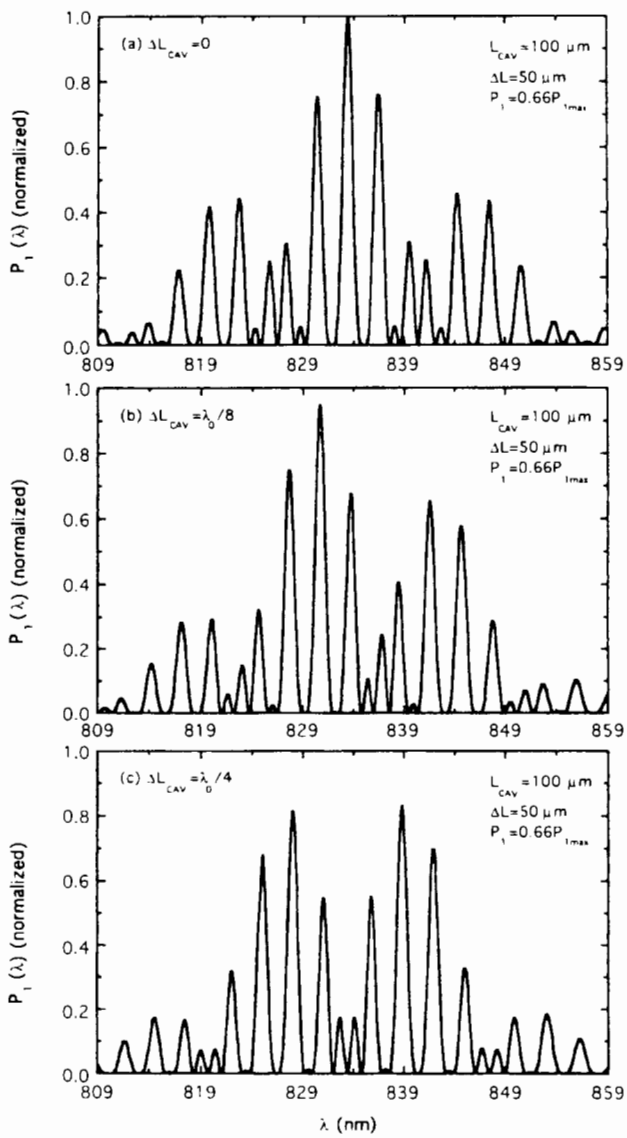

Figure 3. Normalized representation of term A of $P_1(\lambda)$ in equation (11) when $\Delta L = 50$ μm for three different situations: (a) $\Delta L_{CAV} = 0$, (b) $\Delta L_{CAV} = \lambda_0/8$; (c) $\Delta L_{CAV} = \lambda_0/4$ (the other parameters are identical to those in figure 2).

We will now calculate the total power reaching detector D_1. The following approximations were made in performing the integration. (i) In equations containing $FBG(\nu)$ it is assumed that $P_S(\nu) = P_S(\nu_B)$ due to the fact that $\Delta\nu_S \gg \delta\nu$. (ii) Exponential terms of the form $\exp[-(L_{CAV}/L_{cFBG})^2]$ are considered unitary since $L_{cFBG} \gg L_{CAV}$. (iii) Expressions containing integrals of the form

$$\int e^{-a\nu^2} \cos b\nu \, d\nu \tag{12}$$

where

$$\frac{b^2}{4a} \approx 8\left(\frac{L_{CAV}}{L_{cA}}\right)^2 \tag{13}$$

$$L_{cA} = \frac{c}{\Delta\nu_F}\sqrt{\frac{2\ln 2}{\pi}} \tag{14}$$

are neglected because it is assumed that the spectrum of the source is sufficiently broad so that the integral extends over many periods of the cosine function, which is true since $L_{CAV} \gg L_{cS}$ (L_{cS} is the coherence length of the light source).

Using these approximations in equation (11) we obtain:

$$P_1 = \frac{k}{8}P_0\left[1 + \frac{1}{2}e^{-\frac{\pi}{2}\left(\frac{2\Delta L_{CAV} - \Delta L}{L_{cS}}\right)^2} \times \cos\left(\frac{2\pi\nu_0}{c}(2\Delta L_{CAV} - \Delta L)\right)\right]$$

$$+ \frac{Rk}{8}\left(-3 + \frac{3R}{\sqrt{2}} - \frac{R^2}{\sqrt{3}}\right)P_0\frac{\delta\nu}{\Delta\nu_S}e^{-4\ln 2\left(\frac{\nu_B - \nu_0}{\Delta\nu_S}\right)^2} \times \left[1 + \cos\left(\frac{2\pi\nu_B}{c}(2L_{CAV} + \Delta L)\right) + \cos\left(\frac{2\pi\nu_B}{c}(2L_{CAV} + 2\Delta L_{CAV})\right)\right]$$

$$+\frac{1}{2}\cos\left(\frac{2\pi\nu_B}{c}(2\Delta L_M-\Delta L)\right)$$
$$+\frac{1}{2}\cos\left(\frac{2\pi\nu_B}{c}(4L_{CAV}+2\Delta L_{CAV}+\Delta L)\right)\Bigg]$$
$$+\frac{R}{16}\left(1-\frac{R}{\sqrt{2}}\right)P_0\frac{\delta\nu}{\Delta\nu_S}\,\mathrm{e}^{-4\ln 2\left(\frac{\nu_B-\nu_0}{\Delta\nu_S}\right)^2}\Bigg[1$$
$$+\cos\left(\frac{2\pi\nu_B}{c}(2L_{CAV}+\Delta L)\right)\Bigg]. \tag{15}$$

In this equation the contributions of each term in equation (11) to the total optical power at D_1 are evident. The first term in equation (15), corresponding to term A in equation (11), is the interferometric signal obtained in a white light tandem interferometer illuminated with a low coherence optical source. From this signal, it is possible to recover the cavity information via two different approaches: visibility measurements and phase measurements. The second term results from illumination of the two interferometers with coherent light, i.e., light with the gratings spectral shape which has a coherence length much larger than that of the cavity and receiving interferometer path-imbalances. The third term in equation (15) comes from light reflected by the sensing grating that reaches the receiving interferometer.

We now focus on our analysis on the first term of equation (15). The effect of the other two terms will be addressed later. As was mentioned before, change in the cavity length can be obtained in two different but complementary approaches. The first approach is based on the continuous monitoring of the fringe visibility via maximizing the exponential factor in the first term of equation (15). The other uses a phase tracking technique by generating a pseudo-heterodyne carrier. In this case, the tandem interferometer has a path-imbalance close to zero. A sawtooth wave induces a phase modulation in the receiver interferometer with an amplitude adjusted to scan over the entire transfer function, resulting in a signal of the form

$$P_1 \approx \frac{k}{8}P_0\left(1+\frac{1}{2}\cos(\omega_c t-\phi_{CAV})\right] \tag{16}$$

where

$$\phi_{CAV}=\frac{4\pi\nu_0}{c}\Delta L_{CAV}+\phi_0 \tag{17}$$

ω_c is the carrier angular frequency and ϕ_0 is a constant phase term. Considering that $\Delta L_{CAV}=\Delta L_M+\Delta L_T$ and $\Delta L_T=\beta\Delta T$, the signal at the output of a phase recovery device can be expressed as

$$\Delta S^1_{CAV}=K^1_{T/CAV}\,\Delta T+K^1_{L/CAV}\,\Delta L_M \tag{18}$$

where index 1 refers to the proposed phase measurement scheme, $K^1_{T/CAV}$ and $K^1_{L/CAV}$ are coefficients related to the system response to temperature variation (ΔT) and mirror displacement (ΔL_M) in the sensing cavity. In the second approach, the visibility of the tandem interferometer is maximized by tuning the receiver interferometer to match its path imbalance to that of the cavity. Therefore, a signal that is proportional to change in the cavity length will be obtained and can be written as,

$$\Delta S^2_{CAV}=K^2_{T/CAV}\,\Delta T+K^2_{L/CAV}\,\Delta L_M \tag{19}$$

where index 2 refers to the visibility measurement technique and the coefficients $K^2_{T/CAV}$ and $K^2_{L/CAV}$ have the same meaning as in equation (18). It is convenient to combine equations (1), (18) and (19) in a single set, i.e.

$$\begin{cases}\Delta S^i_{CAV}=K^i_{T/CAV}\,\Delta T+K^i_{L/CAV}\,\Delta L_M & i=1,2\\ \Delta S_{FBG}=K_{T/FBG}\,\Delta T.\end{cases} \tag{20}$$

For each index i, the correspondent set of two equations gives the possibility of recovering ΔL_M and ΔT from the knowledge of the coefficients K. It is understood that this set of equations is strictly valid in the situation where the response of the sensor to temperature and displacement is linear within the measurement range.

The described phase and visibility approaches are complementary. In other words, the phase measurement technique provides a higher sensitivity and also the capability of a large dynamic range while the visibility technique has the advantages of absolute measurement. The visibility technique is an intrinsically self-referenced method, i.e., the system may be powered OFF and ON during the operation without any loss of continuity. Additionally, this technique may be used for quasi-static parameters over a large dynamic range.

To assess the validity of the proposed sensing topology it is necessary to compare the signals associated with the second and third terms in equation (15) with the signal associated with the first term that contains the information of interest. Among these two terms, the second term is smaller than the third one because it arises from light transmitted through both gratings and also due to the fact that the cavity is low finesse, i.e., the re-injection coefficient k is small. This assumption may be checked by inserting some typical numbers into equation (15). For example, for $R\approx 1$, $k\approx 0.04$, $\nu_B\approx\nu_0$ and $\delta\nu/\Delta\nu_S\approx 0.01$, the ratio of amplitudes of the third term and second term is ≈ 3. Therefore, in the following analysis only the effect of the third term will be addressed.

To simplify the analysis, we will consider the phase measurement approach in the situation when $\nu_B\approx\nu_0$. After neglecting the second term, equation (15) will take the following form,

$$P_1\approx 2C_1+C_2+C_0\cos\left(\omega_c t+\phi^*_{CAV}\right) \tag{21}$$

where

$$C_0=\Bigg[C_1^2+C_2^2+2C_1C_2$$
$$\times\cos\left(\frac{4\pi\nu_0}{c}(L_{CAV}-\Delta L_{CAV})\right)\Bigg]^{1/2} \tag{22}$$

$$\phi^*_{CAV}=\arctan\left[\frac{C_1\sin\left(-\frac{4\pi\nu_0}{c}\Delta L_{CAV}\right)+C_2\sin\left(\frac{4\pi\nu_0}{c}L_{CAV}\right)}{C_1\cos\left(-\frac{4\pi\nu_0}{c}\Delta L_{CAV}\right)+C_2\cos\left(\frac{4\pi\nu_0}{c}L_{CAV}\right)}\right]+\phi_0 \tag{23}$$

$$C_1=\frac{k}{16}P_0$$
$$C_2=\frac{R}{16}\left(1-\frac{R}{\sqrt{2}}\right)P_0\frac{\delta\nu}{\Delta\nu_S}. \tag{24}$$

In the situation where no fiber grating is used in the system, $\delta\nu/\Delta\nu_S = 0$ and equation (21) becomes identical to equation (16). The third term in equation (15) causes a system readout error dependent on ΔL_{CAV} (equation (23)), i.e., $\phi^*_{CAV} \neq \phi_{CAV}$. To quantify the importance of this effect a numerical example will be used. For $\lambda_0 = 833.5$ nm, $L_{CAV} = 100$ μm, $R \approx 1$, $k \approx 0.04$ and $\delta\nu/\Delta\nu_S \approx 0.01$, the maximum error, $|\phi^*_{CAV} - \phi_{CAV}|/\phi_{CAV}$, is smaller than 5%. This is consistent with the ratio of the amplitudes between the first and third terms in equation (15). This error may be reduced by careful selection of parameters R, k and $\delta\nu/\Delta\nu_S$.

3. Experimental

Figure 1 shows the experimental arrangement. The cavity length ($L_{CAV} \approx 100$ μm) was much larger than the coherence length of the light source (Superlum SLD-361/A, $\lambda_0 = 833.5$ nm, $\Delta\lambda_S = 25$ nm, $L_{cS} \approx 18.5$ μm). The cavity was formed between the fiber end and a mirror (see insert figure), with a re-injection coefficient of $k \approx 0.04$ (the efficiency of launching back light into the fiber). An in-fiber Bragg grating was formed very near to the fiber end and it was encapsulated within the Fabry–Pérot cavity. The Bragg grating was fixed to the mechanical structure from just one end in order to ensure that no strain was applied to it. In this configuration, the grating (FBG_S, $\lambda_B = 836$ nm, $\delta\lambda = 0.2$ nm, $R \approx 0.9$, $L_{cFBG} \approx 2.3$ mm) is only affected by temperature change within the cavity. Optical signals from the extrinsic Fabry–Pérot and from the fiber Bragg grating travel back to the detectors via the same optical fiber. The interferometric signal is affected by temperature variations in the cavity (ΔT) and the mirror displacement (ΔL_M), while the spectrum of reflected light from the Bragg grating is only a function of temperature. In the receiving end, a fiber Bragg grating (FBG_R, $\lambda_B = 836$ nm, $\delta\lambda = 0.2$ nm, $R \approx 0.9$, $L_{cFBG} \approx 2.3$ mm) was used in series with a fiber Mach–Zehnder interferometer with an adjustable path imbalance. The receiving grating (FBG_R) was actively tuned, via a longitudinal stretch of fiber, to match its spectral response to that of the sensing grating (FBG_S). This, effectively, gives ΔS_{FBG} in equation (20). A piezoelectric transducer (PZT) was incorporated in one arm of the Mach–Zehnder interferometer as a phase modulator. By applying a sawtooth waveform to the PZT, a pseudo-heterodyne carrier with frequency of 360 Hz was generated at the output of the tandem interferometer. The phase sensitivity of the interferometer to applied voltage to the PZT was $K_{PZT} = 0.23$ rad V^{-1}.

The visibility measurements were performed by adjusting the path imbalance of the receiving interferometer by maximizing the carrier amplitude at Out_1 to obtain ΔS^2_{CAV}. The phase measurements were performed using a lock-in amplifier, which provides ΔS^1_{CAV}.

The coefficients K in equation (20) were experimentally determined by measuring the interferometric phase (or path imbalance) under these two conditions: (i) the temperature of the cavity was varied while no external displacement was applied to the cavity mirror; (ii) the temperature was kept constant while the mirror was displaced.

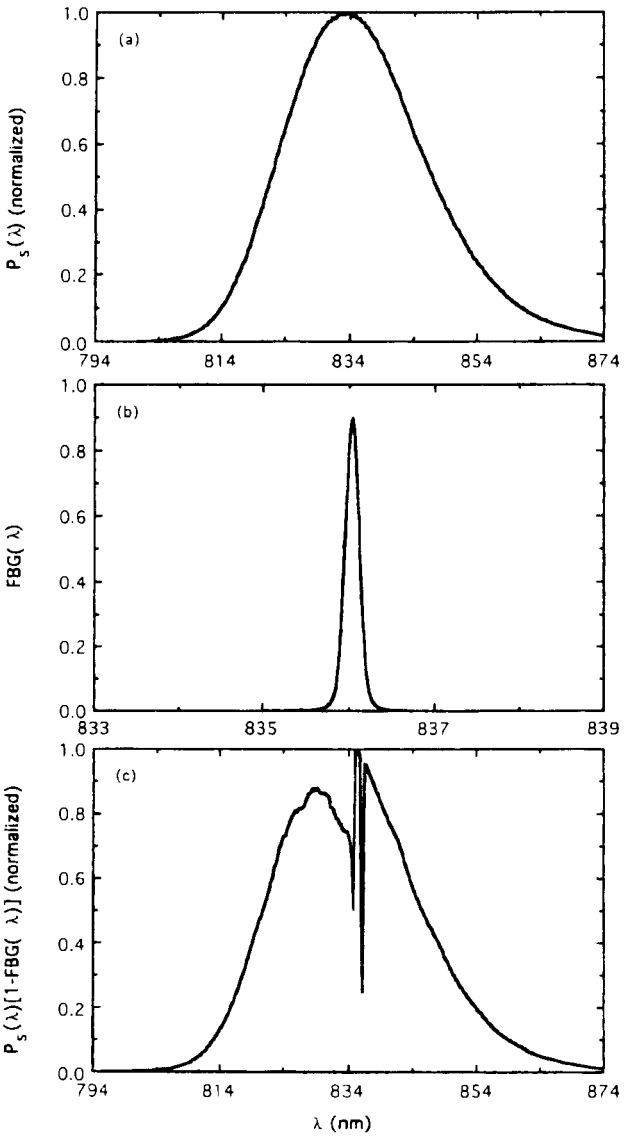

Figure 4. Spectra of (a) the optical source, (b) light reflected from the sensing fiber Bragg grating and (c) light transmitted by the sensing fiber Bragg grating.

4. Results and discussion

In figure 4 the spectra of the optical source, the reflected light and the transmitted light from the sensing fiber Bragg grating are shown. The gratings were of type II [17] and exhibited non-uniform loss over their spectral range (figures 4(b) and (c)). This will result to an extra feature on the channeled spectrum of light arriving at the receiving interferometer

Figure 5 shows the channeled spectrum returned from the sensor head. Lines (a) and (b) represent two cases when ΔL_{CAV} are changed by $\lambda_0/4$ relative to each other, corresponding to a phase variation in the cavity of π. It can be observed that the fringes of the spectrum are antiphase, as expected, and that the spectrum reflected by the fiber Bragg grating does not change between the two cases. This feature was predictable because the sensor head was built in such a way that the Bragg wavelength is only temperature dependent, the parameter that did not change between the two experimental cases.

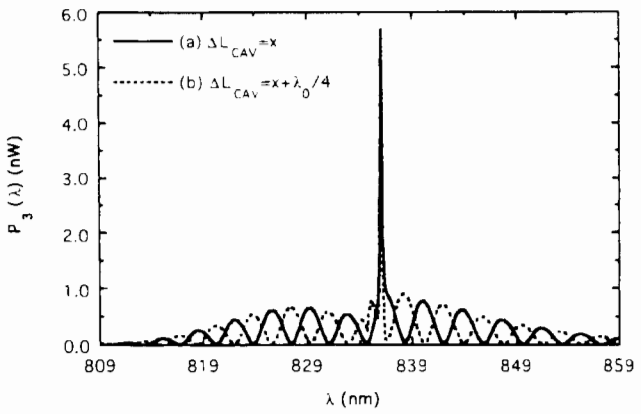

Figure 5. Spectrum of the light returned from the sensor head (measured at Out_3 in figure 1). Between the two cases presented ΔL_{CAV} was changed by $\lambda_0/4$.

Figure 6 shows the light spectrum at Out_1 when $\Delta L = 0$. Two general features are observable: first, the spectral signature of the sensing fiber Bragg grating is not present because it has been removed by the receiving fiber Bragg grating; second, the amplitude of the channeled spectrum fringes is modulated accordingly. The three parts of figure 6 are associated with $\Delta L_{CAV} = 0$, $\Delta L_{CAV} = \lambda_0/8$ and $\Delta L_{CAV} = \lambda_0/4$, respectively. The first one corresponds to the case when the transfer function of the cavity is adjusted in period and in phase to the transfer function of the receiving interferometer, resulting in spectral fringes with maximum amplitude and leading to a maximum value of power in Out_1 (P_{1max}). The second one is an intermediate case ($P_1 = 0.84P_{1max}$) and the third one is associated with the situation in which the two transfer functions are adjusted in period and opposite in phase, resulting in spectral fringes with minimum amplitude and giving a minimum value for P_1 ($0.69P_{1max}$). From these values of P_1, the fringe visibility of the tandem interferometer is calculated as ≈ 0.2. This value was also confirmed by direct measurement of the visibility of the interferometric signal at Out_1. It must be mentioned that this value is smaller than 1/2 (the largest value possible) due to the fact that the power at the two arms of the receiving interferometer was different and, also due to polarization state mismatch between the two interfering waves.

Figure 7 shows the spectrum of light in Out_1 when $\Delta L = 50\ \mu m$. This means that the cavity and receiving interferometer transfer functions have different spectral periodicity, resulting in similar values for average power P_1 in the three situations considered: (a) $\Delta L_{CAV} = 0$, $P_1 = 0.68P_{1max}$; (b) $\Delta L_{CAV} = \lambda_0/8$, $P_1 = 0.66P_{1max}$ and (c) $\Delta L_{CAV} = \lambda_0/4$, $P_1 = 0.68P_{1max}$. This behavior arises from the fact that the path imbalance of the tandem interferometer is significantly larger than the coherence length of the light source, resulting in a low level of interference. When figures 6 and 7 are compared with figures 2 and 3, a fair agreement is observable, which favorably validates the theoretical analysis presented in section 2.

The results presented in figures 8(a)–(c) show a linear response to temperature change and displacement for the

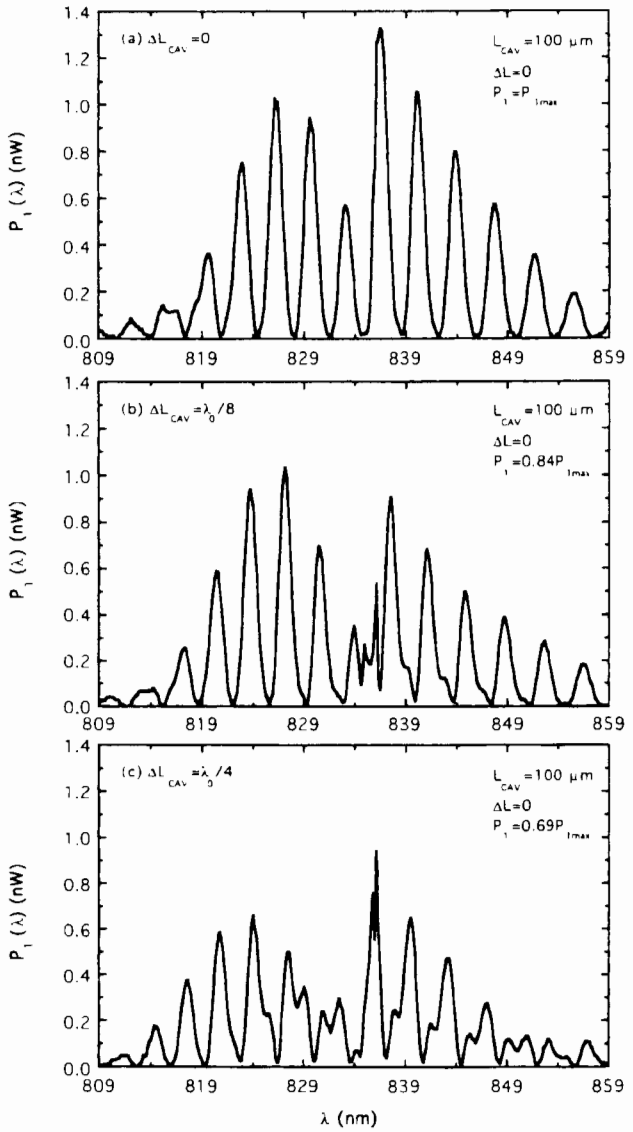

Figure 6. Spectrum of the light at Out_1 when $\Delta L = 0$ for three different situations: (a) $\Delta L_{CAV} = 0$; (b) $\Delta L_{CAV} = \lambda_0/8$; (c) $\Delta L_{CAV} = \lambda_0/4$.

cavity and a linear response to temperature change for the Bragg sensor. Results presented in figures 8(a) and (b) were obtained using the phase measurement technique and data shown in figure (c) correspond to a Bragg wavelength shift of ≈ 8.1 pm $^{\circ}C^{-1}$. This linear behavior supports our initial assumption that resulted in equation (20). From these experimental data, the displacement and thermal coefficients of the cavity and thermal coefficient of the fiber grating were calculated as

$$\begin{aligned} K^1_{T/CAV} &= 23.40 \pm 0.37 \text{ rad } ^{\circ}C^{-1} \\ K^1_{I/CAV} &= 15.04 \pm 0.13 \text{ rad } \mu m^{-1} \\ K_{T/FBG} &= 2.274 \pm 2.4 \times 10^{-2} \ \mu m\ ^{\circ}C^{-1}. \end{aligned} \tag{25}$$

Substitute these coefficients in equation (20) and take the inverse of the coefficients matrix to obtain the following equation:

$$\begin{bmatrix} \Delta T \\ \Delta L_M \end{bmatrix} = \begin{bmatrix} 0 & 0.44 \\ 6.6 \times 10^{-2} & -0.68 \end{bmatrix} \begin{bmatrix} \Delta S^1_{CAV} \\ \Delta S_{FBG} \end{bmatrix}. \tag{26}$$

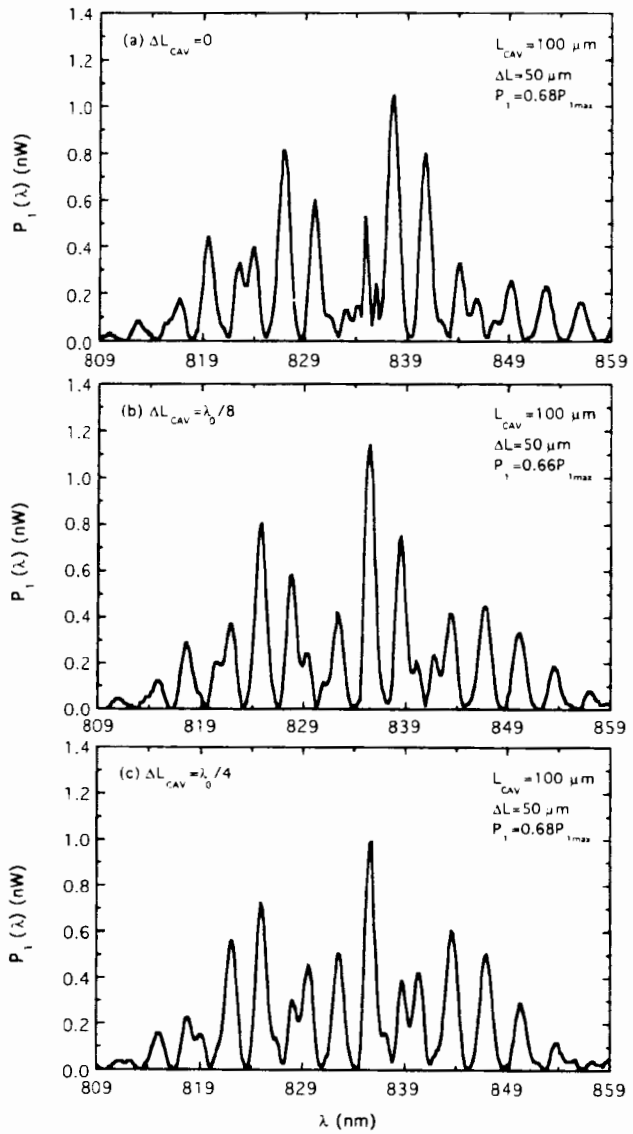

Figure 7. Spectrum of light in Out_1 when $\Delta L = 50\ \mu m$ for three different situations: (a) $\Delta L_{CAV} = 0$; (b) $\Delta L_{CAV} = \lambda_0/8$; (c) $\Delta L_{CAV} = \lambda_0/4$.

This simple and attractive form was achieved since the coefficients matrix that generates equation (20) is well conditioned with a determinant of ≈ 34 rad $^{\circ}C^{-1}$.

To assess the validity of equation (26), we simultaneously changed the temperature of the sensor by 5.1 °C and displaced the mirror by 1.34 μm. The temperature and displacement were then measured with our sensor using equation (26) as $\Delta T = 5.3\ ^{\circ}C$ and $\Delta L_M = 1.23\ \mu m$. This corresponds to a deviation of $\approx 4\%$ for temperature and $\approx 8\%$ for displacement from the actual values.

The results presented in figure 9 were obtained from the visibility measurement technique. Using a procedure similar to the one described above, the following coefficients were calculated:

$$K^2_{T/CAV} = 3.07 \pm 0.02\ \mu m\ ^{\circ}C^{-1}$$
$$K^2_{L/CAV} = 2.02 \pm 0.05\ \mu m\ \mu m^{-1} \qquad (27)$$
$$K_{T/FBG} = 2.274 \pm 2.4 \times 10^{-2}\ \mu m\ ^{\circ}C^{-1}.$$

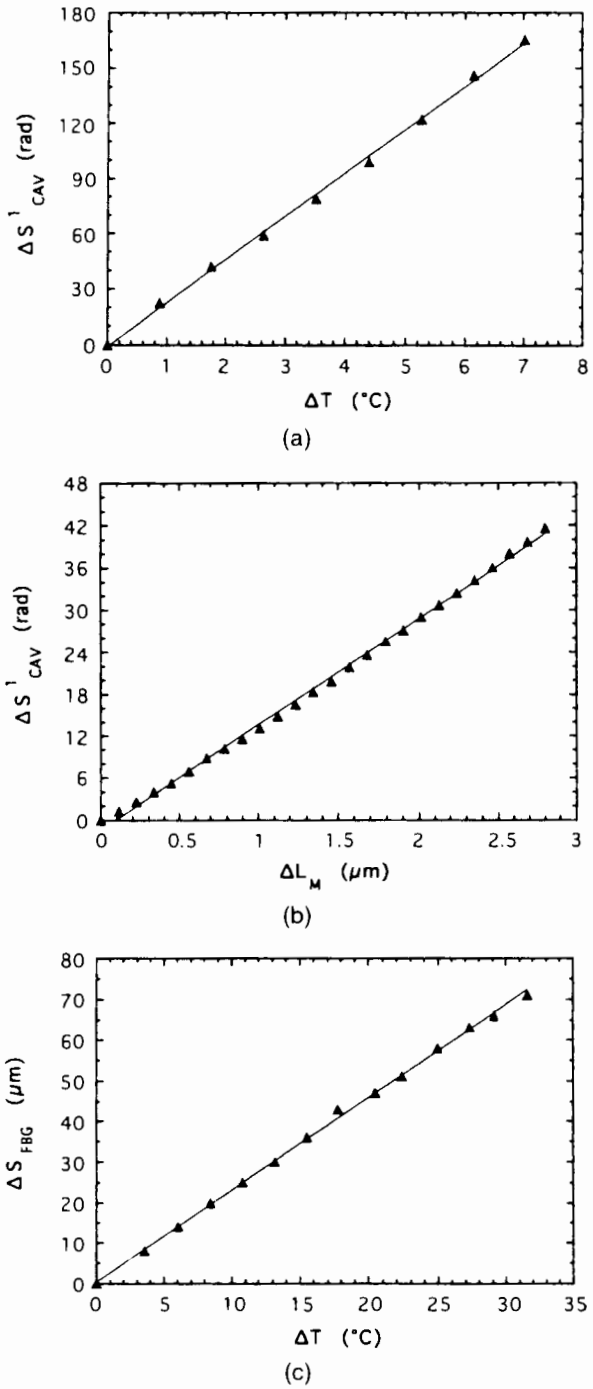

Figure 8. Temperature-induced phase change with no applied displacement to the cavity mirror; (b) displacement-induced phase change with the cavity at constant temperature; (c) elongation of the fiber containing the FBG_R required to keep it tuned to the FBG_S when the sensor temperature changes.

From these coefficients and following a procedure similar to the one employed to obtain equation (26) gives:

$$\begin{bmatrix} \Delta T \\ \Delta L_M \end{bmatrix} = \begin{bmatrix} 0 & 0.44 \\ 0.50 & -0.67 \end{bmatrix} \begin{bmatrix} \Delta S^2_{CAV} \\ \Delta S_{FBG} \end{bmatrix}. \qquad (28)$$

Again, the coefficients matrix that generates equation (20) is well conditioned with a determinant of $\approx 4.6\ \mu m\ ^{\circ}C^{-1}$. This result was tested by simultaneously changing the temperature of the sensor by 16.2 °C and displacing the mirror by 20.3 μm. A temperature change of

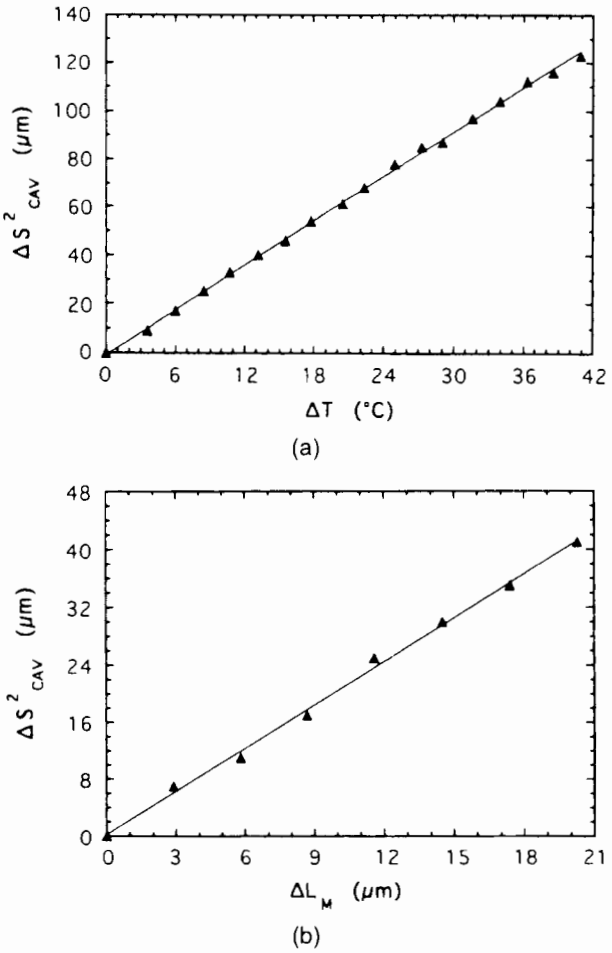

Figure 9. Results obtained using the visibility measurement technique: (a) temperature-induced response of the sensor with no applied displacement to the cavity mirror; (b) displacement-induced response of the sensor with the cavity at constant temperature.

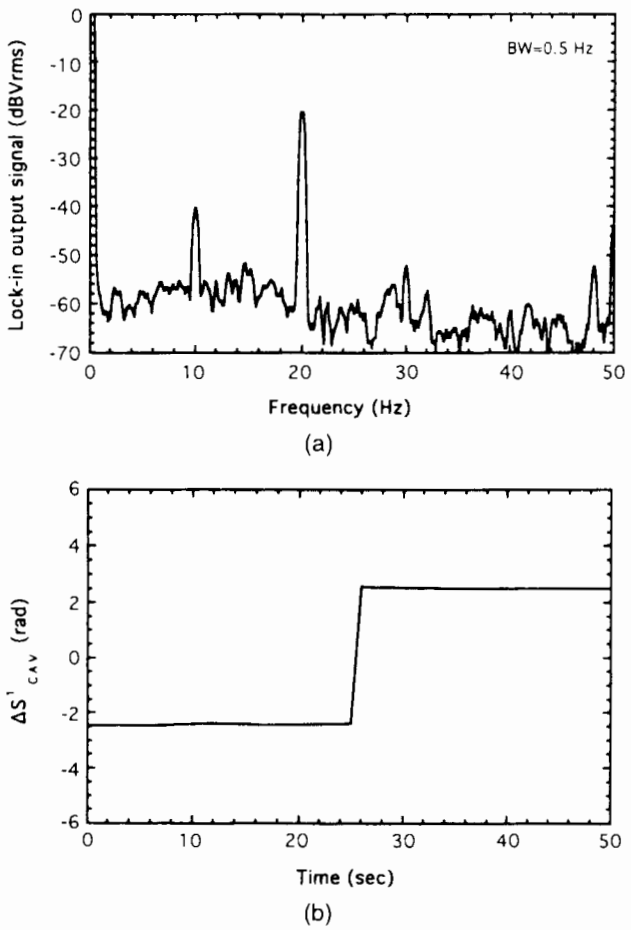

Figure 10. Output of the phase measurement set-up when: (a) a signal with amplitude of 4.4 nm at 20 Hz is applied to the cavity mirror; (b) the position of the cavity mirror is stepped by 336 nm.

$\Delta T = 17.2\,^{\circ}\mathrm{C}$ and displacement of $\Delta L_M = 21.0\ \mu\mathrm{m}$ were measured by the sensor using equation (28), resulting in errors of ≈6% and ≈3%, respectively. These results indicate that the proposed sensor can be used to discriminate the effects of temperature and displacement in the cavity. The measurement errors were caused primarily by temperature effects on the Mach–Zehnder interferometer and in the receiving fiber Bragg grating (FBG_R).

The sensitivity of the cavity to displacement, at constant temperature, and to temperature, with no displacement, were determined using the phase measurement technique as ≈0.7 nm $Hz^{-1/2}$ and ≈4.3×10^{-4} °C $Hz^{-1/2}$, respectively at a frequency of ≈100 mHz (a quasi-static case). However, when temperature was varied and the effect was compensated by the fiber Bragg grating the measurement accuracy was a few percent as discussed earlier. The dynamic sensitivity of the sensor was obtained by applying a signal with an amplitude of 4.4 nm at 20 Hz to the cavity mirror via a PZT. The resulting signal-to-noise ratio observed when the lock-in output signal was applied to a spectrum analyzer (figure 10(a)) was ≈43 dB for a bandwidth of 0.5 Hz, giving a dynamic displacement sensitivity of ≈0.04 nm $Hz^{-1/2}$. Figure 10(b) illustrates the static sensitivity of the sensor. It shows the output of the lock-in for two different values of the interferometric phase during a time interval of 50 s. From the observable fluctuations, a value of 6.1 nm $Hz^{-1/2}$ can be estimated for the sensor static sensitivity. It must be noted that this value depends on phase fluctuations that are environmentally coupled to the receiving interferometer during the measurement. Therefore, proper shielding could significantly improve this result. It should also be emphasized that the accuracy in determining coefficients K in equation (20) will be, in most practical cases, the limiting factor of the system accuracy because of the error propagation in the matrices of equations (26) and (28) [18]. Therefore, special care must be employed in the process of obtaining those coefficients.

5. Conclusion

In this paper we presented a new sensor design based on the utilization of white light interferometry and a fiber Bragg grating that allows simultaneous measurement of temperature and displacement. The sensor uses an embedded fiber Bragg grating and an extrinsic Fabry–Pérot cavity. The Fabry–Pérot cavity has a high displacement resolution and the grating measures the local temperature and provides a reference to compensate for the thermal

sensitivity of the cavity. The experimental results demonstrated that this sensor design is practical and with proper selection of design parameters one can tailor this system for a particular application. The theoretical model presented in this paper accurately predicts the characteristic of the system, therefore, it can be used for system optimization.

Acknowledgments

L A Ferreira and A B Lobo Ribeiro acknowledge financial support from Programa PRAXIS XXI. This work was in part supported by NSF grant DMI-9413966.

References

[1] Chen S, Palmer A W and Grattan K T V 1993 A study of the characteristics of connected optical fiber Fabry–Pérot cavities *Pure Appl. Opt.* **2** 429–35

[2] Lee C E and Taylor H F 1991 Fiber-optic Fabry–Pérot temperature sensor using a low-coherence light source *J. Lightwave Technol.* **LT-9** 129–34

[3] Rao Y J, Jackson D A, Jones R and Shannon C 1994 Development of prototype fiber-optic-based Fizeau pressure sensors with temperature compensation and signal recovery by coherence reading *J. Lightwave Technol.* **LT-12** 1685–95

[4] Rao Y J and Jackson D A 1996 Universal fiber-optic point sensor system for quasi-static absolute measurements of multiparameters exploiting low coherence interrogation *J. Lightwave Technol.* **LT-14** 592–9

[5] Farahi F, Webb D J, Jones J D C and Jackson D A 1990 Simultaneous measurement of temperature and strain: cross sensitivity considerations *J. Lightwave Technol.* **LT-8** 138–42

[6] Vengsarkar A, Michie W, Jankovic L, Culshaw B and Claus R 1990 Fiber optic sensor for simultaneous measurement of temperature and strain *SPIE* **1367** 249–60

[7] Singh H and Sirkis J 1996 Simultaneous measurement of strain and temperature using optical fiber sensors: two novel configuration *Proc. OFS '96 (Sapporo, Japan)* pp 108–11

[8] Morey W W, Meltz G and Weiss J M 1992 Evaluation of a fiber Bragg grating hydrostatic pressure sensor *Proc. OFS '92 (Monterey, USA)* Post deadline paper PD-4.4

[9] Xu M G, Archambault J-L, Reekie L and Dakin J P 1994 Discrimination between strain and temperature effects using dual-wavelength fiber grating sensors *Electron. Lett.* **30** 1085–7

[10] Michie W C, Culshaw B, Roberts S S J and Davidson R 1991 Fiber optic technique for simultaneous measurement of strain and temperature variations in composite materials *Proc. SPIE* **1588** 342–55

[11] Gerges A S, Farahi F, Newson T P, Jones J D C and Jackson D A 1988 Fiber-optic interferometric sensors using a low coherence source: dynamic range enhancement *Int. J. Optoelectron.* **3** 311–22

[12] Measures R M, Alavie A T, Maaskant R, Ohn M, Karr S and Huang S 1995 A structurally integrated Bragg grating laser sensing system for a carbon fiber prestressed concrete highway bridge *Smart Mater. Struct.* **4** 20–30

[13] Sirkis J 1993 A unified approach to phase–strain–temperature models for smart structure interferometric optical fiber sensors: part 2 applications *Appl. Opt.* **32** 762–73

[14] Measures R M 1993 Fiber optic sensing for smart composite structures *Composite Eng.* **3** 715–50

[15] Fuhr P L, Huston D R, Kajenski P J and Ambrose T P 1992 Performance and health monitoring of the Stafford medical building using embedded sensors *Smart Mater. Struct.* **1** 63–8

[16] Udd E (ed) 1995 *Fiber-optic Smart Structures* (New York: Wiley)

[17] Bennion I, Williams J A R, Zhang L, Sugden K and Doran N J 1996 UV-written in-fiber Bragg gratings *Opt. Quantum Electron.* **28** 93–135

[18] Jin W, Michie W C, Thursby G, Konstantaki M and Culshaw B 1991 Simultaneous measurement of strain and temperature error analysis *Proc. SPIE.* **1588** 342–55